Noise-Guided Transport for Imitation Learning

Lionel Blondé[1]* **Joao A. Candido Ramos**[1,2] **Alexandros Kalousis**[1]

[1]HES-SO Geneva   [2]University of Geneva, Switzerland

Abstract

We consider imitation learning in the low-data regime, where only a limited number of expert demonstrations are available. In this setting, methods that rely on large-scale pretraining or high-capacity architectures can be difficult to apply, and efficiency with respect to demonstration data becomes critical. We introduce Noise-Guided Transport (NGT), a lightweight off-policy method that casts imitation as an optimal transport problem solved via adversarial training. NGT requires no pretraining or specialized architectures, incorporates uncertainty estimation by design, and is easy to implement and tune. Despite its simplicity, NGT achieves strong performance on challenging continuous control tasks, including high-dimensional Humanoid tasks, under ultra-low data regimes with as few as 20 transitions. Code is publicly available at: `https://github.com/lionelblonde/ngt-pytorch`.

1 Introduction

The recent advent of pretrained, internet-scale vision–language models has made supervised learning techniques like behavioral cloning (BC) [47] viable for imitation learning (IL) in the very large data regime [12, 6], i.e. when tens of thousands of state-actions pairs are available. Yet, **in low-data regimes** where only a handful of expert demonstrations are available, BC often fails to generalize. *This challenge is common in **healthcare applications** such as human gait analysis from impaired patients, where acquiring diverse, high-quality demonstrations is constrained by patient availability and clinical variability.* Limited diversity in demonstration data often leads BC to accumulate compounding errors at test time [52]. In this work, we devise a sample-efficient method for IL [5] to address scenarios with scarce expert data.

Apprenticeship learning [1]—inverse RL (IRL) in an inner loop; RL in an outer loop—is shielded from the compounding errors BC suffers from. Yet, IRL is tedious because it is ambiguous. This ambiguity was identified by Ziebart et al. [66] and solved with maximum entropy IRL (MaxEnt IRL). Finn et al. [18] later showed that GANs [21] solve the same objective as MaxEnt IRL. These observations align

Figure 1: Performance of a subset of methods, aggregated over tasks and number of demonstrations. Humanoids not included.

with the sustained success of GAIL [28] in IL. Given our focus on sample efficiency—in terms of expert dataset size but also interactions with the world—we turn to the off-policy evolution of
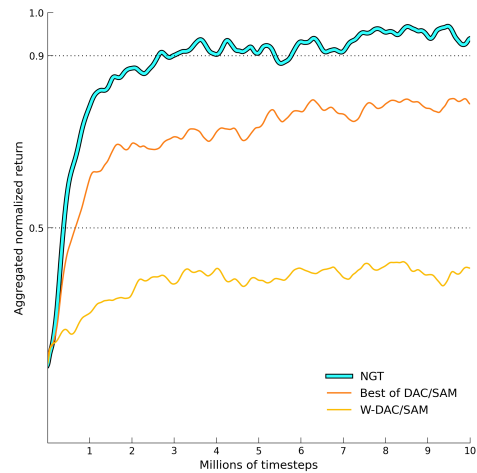
---

*Correspondence to: `mail@lionelblonde.com`

GAIL, specifically DAC [37] and SAM [7]. Inheriting from GANs, these adversarial IL approaches minimize the JS-divergence between the expert and the agent by using a binary classifier that is trained to discriminate between their respective state-action distributions.

While adversarial IL has been extended to other divergences and distances [20, 34], these approaches typically begin by selecting a divergence and fitting it into a predefined framework. In contrast, we start from the core desideratum: constructing a reward function that distinguishes expert from agent. In SECTION 4, we derive our objective from first principles, formulating reward learning as a problem of pseudo-density estimation from random priors [44]. We show that this learning objective coincides with an earth-mover distance, a metric grounded in optimal transport (OT) theory [59]. We refer to our method as **Noise-Guided Transport (NGT)**. We also provide guarantees for the loss optimized in practice, showing how its deviation from the true objective concentrates with sample size.

Finally, in SECTION 5, we empirically evaluate and compare NGT in the low-data regime against a diverse set of baselines, including OT-based methods and a diffusion-based AIL method [60]. We benchmark the methods on standard continuous control tasks for low-data imitation learning. Notably, we include Humanoid locomotion: a high-dimensional, challenging control task that is rarely addressed in this regime due to its complex dynamics and large state-action space. Despite this, NGT successfully learns to perform humanoid locomotion. Among the baselines, only a diffusion-based approach is able to make progress on this task, albeit sub-optimally and with greater computational overhead. A key ingredient in NGT's success is the use of distributional losses [32] in reward learning, which contribute to its robustness in such difficult environments. Moreover, in FIGURE 3, we show NGT's performance across varying levels of demonstration availability, under various subsampling rates, showing how it scales with data—from *as few as 20 transitions*. FIGURE 3 also includes results in the **state-only setting**, where expert actions are not available. Overall, our results demonstrate that NGT scales gracefully with both task complexity and data scarcity, all while remaining lightweight. As a result, **it emerges as a highly sample-efficient method that shines in the low-data regime**.

2 Related Works

DAC and SAM [37, 7] have gained recognition for their sample efficiency and simplicity. These methods frame imitation learning as minimizing a divergence between the agent and expert distributions, in line with the original GAN formulation [21]. This divergence minimization can be interpreted through the lens of optimal transport (OT), both in its primal and dual formulations. PWIL [16] approximates the primal form of the EMD with an iterative procedure, while methods like ROT [25] and MAAD [49] use the Sinkhorn algorithm—solving an entropy-regularized approximation of the EMD in the primal formulation—to match full trajectories. In contrast, the dual formulation approximates OT by learning the Kantorovich potentials using neural networks, as done in the adversarial training setup of WGAN [3]. *In NGT, we adopt an OT perspective in its dual form.* When actions are unavailable, sample-efficiency has been mostly tackled by regularization of pre-existing methods. MAAD [49] is an on-policy method that improves on GAIL [28], while OPOLO [65] is an off-policy method that improves on DAC [37]. *In NGT, we do not require such extra regularization.*

AILBoost [10] adopt an orthogonal strategy by enhancing DAC through boosting, a classic ensemble learning technique. In contrast, *NGT incorporates an inner task centered on predicting a diverse set of random priors* [44]. Taken together, these predictions can also be interpreted as a form of ensemble learning, albeit through a fundamentally different mechanism. Prediction tasks based on random priors have proven effective for pseudo-density estimation (PDE). PDE from random priors has been used to learn a *novelty* detector that guides exploration in online RL—an approach called Random Network Distillation (RND) [9]. PDE from random priors has also been used to learn an *expert* detector that guides imitation in offline IL. This approach is called Random Expert Distillation (RED) [61]. PDE could also be geared towards out-of-distribution (OOD) avoidance, also called anti-exploration, in offline RL. Notably, Rezaeifar et al. [51] reports that RND is ineffective for anti-exploration in continuous control tasks in offline RL [51]. However, later findings [43] showed that it performs well when the predictor and prior networks use specific asymmetric architectures that learn separate representations for states and actions before merging them. In this work, we demonstrate that *NGT can leverage random priors* for continuous control *beyond feature engineering*. Ciosek et al. [14] provides theoretical grounding for RND, analyzing concentration properties that characterize the conditions under which the difference between the prior and predictor vanishes. We expand on related works further in APPENDIX D.

3   Background and Setting

We consider an agent that interacts with a Markov Decision Process (MDP) $(\mathbb{S}, \mathbb{A}, P, r, \gamma)$. $\mathbb{S}$ and $\mathbb{A}$ denote the state and action spaces, P the transition dynamics, r the reward function, and $\gamma \in [0, 1)$ the discount factor. We work in the episodic setting, where γ resets to 0 upon episode termination, reflecting finite-horizon rollouts up to T. A policy $\pi(a|s)$ maps states $s \in \mathbb{S}$ to distributions over actions $a \in \mathbb{A}$, aiming to maximize cumulative rewards. Our objective is to learn a policy π that mimics the behavior of an expert, without access to r. Instead, the agent learns from a demonstration dataset $\mathcal{E}$, typically comprising trajectories $\{(s_t, a_t)\}_{t=1}^{T}$. When only states are available (*i.e.*, no actions), the problem reduces to identifying a policy that reproduces expert-like state distributions.

4   Method and Guarantees

Our method comprises an actor-critic architecture [15]—a policy or actor π_θ, and a action-value or critic Q_ω, learned by generalized policy improvement [55]—and a reward model r_ξ. The three functions are modeled with neural networks, with parameters θ, ω, and ξ. The reward model provides the agent with reinforcement signal, and is the sole source of feedback for the decision made by the policy. The critic's purpose is to assign proper credit to those decisions, given the situation the agent is in; it learns the *value* of actions. To do so, the critic posits that feedback can be delayed over the course of an episode and learns to represent the expected future return from that decision onward until the episode ends. All three are learned in an off-policy fashion. This trait is supported by a replay buffer, enabling the agent to replay past experiences [40]. Our goal is for our agent to learn a robust reward signal, from a set of demonstrations that we want our agent to imitate. The input space of the reward model r_ξ can be $\mathbb{S} \times \mathbb{A}$, but also $\mathbb{S} \times \mathbb{S}$ (*state-state* case) or $\mathbb{S}$ (*state-only* case). We will use $\mathbb{X}$ to denote any of these options. P_{expert} denotes the probability distribution of expert data over $\mathbb{X}$, and P_{agent} the one described by the agent. $P(\mathbb{X})$ denotes an arbitrary distribution over $\mathbb{X}$. π_θ and Q_ω are trained with the **Soft Actor-Critic (SAC)** off-policy algorithm [23]. It learns a stochastic policy. Instead of using the reward from the environment—which our setting prevents access to—SAC uses the reward function r_ξ, whose training loop is interlaced with the training loops of SAC, as laid out in ALGORITHM 1. **We now describe how we learn the reward function r_ξ.**

4.1   Reward Learning: Objective

We now introduce our reward learning objective, deriving an adversarial objective based on the problem of **learning from random priors**. Specifically, we consider a prediction problem where the answer is a *deterministic* function of its inputs. This answer is given by a neural network representing $f_\xi^\dagger : \mathbb{X} \to \mathbb{R}^m$ that is *randomly initialized* and *frozen* immediately after initialization. As such, the output of $f_\xi^\dagger$ is m-dimensional target that depends on the input $x \in \mathbb{X}$ in non-stochastic manner. $f_\xi^\dagger$ is dubbed the *prior* network. Another network, the *predictor* network f_ξ, is a carbon copy of the prior network but is not frozen, i.e. it receives gradients throughout training and updates its parameters via gradient descent. By comparing the outputs of predictor network to the prior network with a loss ℓ, we have at our disposal a task whose complexity can scale depending on several factors: the architecture of the networks, the size of the output embedding, and the traits of the loss ℓ. The predictive statistics of this task capture the **epistemic uncertainty** of the m-sized matching.

Consider this problem, where $P(\mathbb{X})$ is a probability distribution over $\mathbb{X}$:

$$\inf_{\xi} \; \mathbb{E}_{x \sim P(\mathbb{X})} \Big[\ell\big(f_\xi(x), f_\xi^\dagger(x)\big) \Big] \tag{1}$$

By the properties of neural networks, performing gradient descent steps on this problem will, to the limit of representational power, make $\ell\big(f_\xi(x), f_\xi^\dagger(x)\big)$ take lower value on $x \sim P(\mathbb{X})$. This system is therefore able to **act as a *pseudo*-density estimator** of P ("pseudo": it does not integrate to 1).

In effect, optimizing the problem in EQ 1 with P_{expert} as $P(\mathbb{X})$ learns an *expert detector*. Wang et al. [61] learns such a detector, in an offline manner, and formulates an RL reward from it. Albeit sound, it falls short of capturing the expert distribution in practice. We argue that what plagues the method is that: *(a)* the pseudo-density is learned entirely offline, and *(b)* it posits that we only have *positive* signal (guided by P_{expert}), closely resembling one-class classification or positive-unlabeled learning.

In fact, for the overwhelming majority of the agent's learning lifespan, the agent has *sub-optimal* behavior. Its behavior (informed by P_{agent}) could therefore be treated as *negative* signal.

This design position, in the classification analogy, turns *one-class* into *binary* classification. This is a view adopted by adversarial methods that train a reward model as the discriminator of a GAN, which is a binary classifier. The original method, GAIL, was on-policy. It was turned off-policy in DAC/SAM. Methods based on GANs optimize a JS-divergence between distributions P_{expert} and P_{agent}, which suffers from mode collapse and vanishing gradients. This leads to instability or failure to train effectively. As such, they require careful regularization. **In this work, we instead build an adversarial training scheme from the problem of predicting random priors** in $\mathbb{R}^m$. Not only do we descend the gradients of $\ell\big(f_\xi(x), f_\xi^\dagger(x)\big)$ on expert data, we also *ascend* its gradients on agent-generated data. By using h_ξ as a shorthand for $x \mapsto \ell\big(f_\xi(x), f_\xi^\dagger(x)\big)$, the loss $L(\xi)$ becomes:

$$L(\xi) := \mathbb{E}_{x \sim P_{\text{expert}}}\big[h_\xi(x)\big] - \mathbb{E}_{x \sim P_{\text{agent}}}\big[h_\xi(x)\big] \tag{2}$$

In the remainder of this work, we refer to h_ξ as the **potential** function, or simply the potential.

Since minimizing $L(\xi)$ trains h_ξ to assign low values to expert data and high values to agent data, composing it with a monotonically decreasing transform naturally inverts this trend—assigning high values to expert states and low values to agent states. This is exactly the behavior we seek for reward assignment. Accordingly, we define the **reward** as: $r_\xi(x) := \exp\big(-h_\xi(x)\big)$. This choice ensures positivity, bounds the reward between 0 and 1 (the pairing loss ℓ is non-negative), and sharpens the contrast between expert and agent behavior. We discuss the reward numerics further in APPENDIX J.

The loss $L(\xi)$ defines the objective that our reward model ξ seeks to minimize. We derived it from first principles, starting from the core desideratum of distinguishing the expert and agent distributions. In the next section, we show that this loss: *(1)* enables the agent to **provably close the gap** with the expert, and *(2)* enjoys **empirical concentration guarantees** that support its practical effectiveness [2].

4.2 Reward Learning: Theoretical Grounding

In this section, we *(1)* show that the adversarial objective in EQ 2, derived in SECTION 4.1, is equivalent to an objective grounded in optimal transport theory; and *(2)* characterize how tightly its empirical estimate concentrates—in other words, how closely it approximates the *true* objective $L(\xi)$.

We define H_ξ^Λ as the set of potential functions $h_\xi : x \mapsto \ell\big(f_\xi(x), f_\xi^\dagger(x)\big)$ that are Λ-Lipschitz. Formally, $H_\xi^\Lambda := \big\{h_\xi : \mathbb{X} \to \mathbb{R}_+; x \mapsto \ell\big(f_\xi(x), f_\xi^\dagger(x)\big) \mid |h_\xi(x) - h_\xi(x')| \leq \Lambda\, d(x, x'), \forall x, x' \in \mathbb{X}\big\}$ where d is a ground metric over the input space $\mathbb{X}$, and $\Lambda < +\infty$. In particular, we make the following design choice: to train our reward model, we restrict the search for a potential function h_ξ that minimizes $L(\xi)$ to the case where $\Lambda = 1$. That is, we optimize EQ 2 over the space of 1-Lipschitz potentials. Using the formalism above: we look for a function $h_\xi \in H_\xi^1$ that is the infimum of $L(\xi)$.

We observe that:

$$\inf_{h_\xi \in H_\xi^1} \Big[\mathbb{E}_{x \sim P_{\text{expert}}}\big[h_\xi(x)\big] - \mathbb{E}_{x \sim P_{\text{agent}}}\big[h_\xi(x)\big]\Big]$$
$$= -\sup_{h_\xi \in H_\xi^1} \Big(\mathbb{E}_{x \sim P_{\text{agent}}}\big[h_\xi(x)\big] - \mathbb{E}_{x \sim P_{\text{expert}}}\big[h_\xi(x)\big]\Big) = -\text{EMD}(P_{\text{agent}}, P_{\text{expert}}) \tag{3}$$

where EMD is the earth mover's distance between the two distributions. It quantifies the dissimilarity between two distributions, calculating the total effort required to transform (or **transport**) one into the other ($P_{\text{agent}} \to P_{\text{expert}}$). EQ 3 shows that when we update ξ to minimize $L(\xi)$, we update ξ to **maximize** the EMD between the distributions. As a result, descending along the gradients of $L(\xi)$—while ensuring that $h_\xi \in H_\xi^1$—maximizes the discrepancies between P_{agent} and P_{expert}.

In the context of OT, the learned potential function (h_ξ) embodies the Kantorovich-Rubinstein duality by iteratively approximating the optimal *dual* potentials that define the EMD. This approach aligns

---

[2]Under the off-policy regime, the P_{agent} shorthand designates following the off-policy distribution β resulting from sampling experiences uniformly, without loss of generality, from the replay buffer. In effect, β is a mixture of past π_θ updates. The bigger the buffer capacity, the older the oldest policy in the mixture.

with the essence of the dual formulation: encoding the **cost landscape** of the transport problem. While the dual form has two potentials (one per $\mathbb{E}[\cdot]$), we learn only one (h_ξ). Specifically, we use h_ξ for the first expectation, and $-h_\xi$ for the second. This design choice[3] reduces the dual constraint (from the dual formulation of the EMD) into a 1-Lipschitz continuity constraint on the single potential—hence our choice to look for $h_\xi \in H^1_\xi$, thereby ensuring consistency with the *primal* transport problem.

We name our method **Noise-Guided Transport (NGT)** because: *(a)* Minimizing the adversarial reward objective $L(\xi)$ guides $f_\xi(x)$ toward the noise returned by the prior network $f^\dagger_\xi(x)$ on expert data while pushing it away on agent data; *(b)* The objective is equivalent to optimizing an OT metric.

In APPENDIX E, we discuss how NGT relates to the problem formulated by [3].

Concentration.   To support the reliability of our reward learning objective $L(\xi)$ in EQ 2, we derive a concentration bound for its empirical estimate $\hat{L}(\xi)$, computed from finite samples drawn from the expert and agent distributions. The result shows that $\hat{L}(\xi)$ converges to its expected value $L(\xi)$ at an exponential rate, with deviation controlled by the Lipschitz constant of the potential and the diameter of the input space. This bound quantifies the sample efficiency of our method and ensures that the empirical loss provides a reliable approximation of the true objective, providing theoretical control over generalization from finite samples. We present the full analysis and proof in APPENDIX F.

4.3   Reward Learning: Practical Execution

In order for the potential $h_\xi : x \mapsto \ell\big(f_\xi(x), f^\dagger_\xi(x)\big)$—central to our reward design (SECTION 4.1)—to satisfy the equivalence laid out in EQ 3 (SECTION 4.2), it must be 1-Lipschitz: $h_\xi \in H^1_\xi$. Thus, we now examine how the Lipschitz constant of h_ξ is governed by the Lipschitz properties of its constituent functions; namely,the predictor and prior networks f_ξ and $f^\dagger_\xi$, and the pairing function ℓ.

Theorem 4.1 (Lipschitz constant of h_ξ). *Let $\Lambda(\cdot)$ denote the Lipschitz constant of a given function. By construction, h_ξ is $\Lambda(h_\xi)$-Lipschitz continuous w.r.t. a ground metric d over $\mathbb{X}$ with, $\forall x_1, x_2 \in \mathbb{X}$:*

$$\Lambda(h_\xi) = \Lambda(\ell)\big(\Lambda(f_\xi) + \Lambda(f^\dagger_\xi)\big) \tag{4}$$

as Lipschitz constant.

We provide the proof of TH 4.1 in APPENDIX G. Having characterized in THEOREM 4.1 how the Lipschitz constant of the potential function h_ξ depends on those of f_ξ, $f^\dagger_\xi$, and ℓ, we now turn to *the practical question* of how to ensure that the condition $h_\xi \in H^1_\xi$ is satisfied—that is, *how* to ensure that $\Lambda(h_\xi) \leq 1$ holds *in practice* over $\mathbb{X}$. The following subsections describe the specific design choices we make, at the architectural and loss function levels[4], to enforce this property in our method.

4.3.1   Controlling the values of $\Lambda(f_\xi)$ and $\Lambda(f^\dagger_\xi)$

EQ 4 shows that $\Lambda(f_\xi)$ and $\Lambda(f^\dagger_\xi)$ compound additively, and their sum compounds multiplicatively with $\Lambda(\ell)$. Therefore, ℓ can still act as a soft gate or low-pass filter that could prevent occasional spikes upstream and thereby cause destructive updates of the reward model. Importantly, $\Lambda(\ell)$ is fixed and does not change with ξ updates—although it could be made to follow a schedule or heuristic. The same goes for $\Lambda(f^\dagger_\xi)$, since the prior network is never updated after initialization. As a result, $\Lambda(\ell)$ and $\Lambda(f^\dagger_\xi)$ depend only on design choices, while $\Lambda(f_\xi)$ can be altered during training. In practice, we do not aim for the *perfect*-1 Lipschitz constant $\Lambda(h_\xi)$, i.e. $h_\xi \in H^1_\xi$; We have found that it is empirically enough to tame its value and keep it "close enough to 1" so as to avoid surges and spikes. We use *spectral normalization* (SN) [42] on every linear layer of the predictor f_ξ and prior $f^\dagger_\xi$, which constrains their Lipschitz constant by maintaining *unit* spectral norm. It is then the choice of non-linearity[5] in f_ξ and $f^\dagger_\xi$ that dictates how their Lipschitz constants deviates from 1.

---

[3]A similar design choice was made by [3] (the EMD is the Wasserstein-1 distance).

[4]We refer the reader to the extensive **ablation studies** presented in APPENDIX N.

[5]Anil et al. [2] discusses how the choice of activation impacts whether the function approximator *can actually* be Lipschitz continuous when one encourages it to be via regularization.

Given that the prior $f_\xi^\dagger$ is frozen after being initialized, *how* the networks are initialized is crucial. We use *orthogonal initialization* (OI) [53, 30] in every layer , which ensures that the weight matrix is a norm-preserving linear transformation. It ensures an even spread in the feature space, avoiding redundancies (reducing correlations) in output space. Since the prior network is never updated and is initialized with OI, it has two appealing traits. *(a)* The random priors—output embedding of $f_\xi^\dagger$—are the result of a full-rank map, and therefore *maximally utilize* the available dimensions m in the output embedding. *(b)* The linear layers already have unit singular values (orthogonal matrix). The highest singular value is therefore already 1: applying SN has no effect, and would not be needed for the prior network. So, with OI and reasonably linear-like activations (e.g. ReLU, LeakyReLU), $\Lambda(f_\xi^\dagger)$ should be close to unit. Using SN is however required for the predictor. Otherwise, $\Lambda(f_\xi)$ can adopt an erratic behavior as ξ gets updated. **Importantly, we did not need to regularize the predictor with a gradient penalty** (GP) [22], while it is *needed* for every single off-policy adversarial IL SOTA baseline (see SECTION 5) [6]. This makes **NGT cheaper and faster** than its counterparts on that front. Indeed, GP is more computationally expensive than SN. GP effectively doubles the cost of the backward pass, while SN only adds minimal overhead.

4.3.2 Controlling the value of $\Lambda(\ell)$

What about $\Lambda(\ell)$? An obvious choice of loss with $\Lambda(\ell) \leq 1$ is the L_1 loss, or better yet, the Huber loss with parameter $\delta = 1$. In fact, most of the losses borrowed from robust regression are 1-Lipschitz and would satisfy our regularity desideratum. The Huber loss turned out to be an excellent option, and it acted as default in our experiments. Notably, NGT allows for the comparison of the embeddings $f_\xi^\dagger$ and f_ξ directly, but they could also be pipped through another map or transform, e.g. learned feature map (see discussion in APPENDIX D), or a non-learned deterministic proxy function. We have tried the latter by wrapping both output embeddings with a softmax. In effect, comparing the softmaxes of embeddings evaluates the similarity between the distribution of output units[7]. We have found that this design choice gave comparable results to the Huber loss, and could give a slight edge in certain tasks.

These losses yielded excellent results, as reported in SECTION 5, with the exception of the Humanoid tasks, where none of the above losses produced satisfactory performance. We expanded the capabilities of NGT by enabling the use of **distributional losses**—specifically, the **histogram loss, Gaussian type**—which were originally introduced for *value learning* in RL [32]. We denote the loss with ℓ_{HLG}. It depends on four hyper-parameters, (a, b, N, σ), where $[a, b]$ is the interval to partition into N bins, and σ dictates the spread of the Normal distribution involved in ℓ_{HLG}. We opted for ℓ_{HLG} (regression $\rightarrow$ classification) because: *(a)* Spreading probability mass to neighboring locations reduces overfitting (label smoothing, [56]); *(b)* Exploiting the ordinal structure of the regression enhances generalization across a range of target values; *(c)* Classification losses have proved to produce better representations and have demonstrated greater robustness to non-stationarity. Turning regression into classification has enabled deep RL to finally reap benefits from scale [24, 26, 17]. This aligns with the "scaling law" paper of Kaplan et al. [33], which demonstrated how well cross-entropy scales. As we show in SECTION 5, ℓ_{HLG} allowed us to successfully scale NGT to the Humanoid tasks.

Distributional losses such as ℓ_{HLG} were originally introduced in the context of value learning, where the targets are scalar values and the model predicts a probability distribution over N discrete bins. In our case, we repurpose this loss for **reward learning**, where the learning signal comes from predicting a vector of m-dimensional random priors. As a result, the prediction is effectively over $N \times m$ bins, rather than N bins. This induces an *architectural asymmetry* between f_ξ and $f_\xi^\dagger$: while the prior network $f_\xi^\dagger$ returns m scalar targets, the predictor f_ξ must now produce an output of size $N \times m$, representing a distribution over bins for each prior dimension. No other loss considered in this work introduces such an asymmetry. We describe the mechanism of ℓ_{HLG} in detail in APPENDIX B, including how we extend the original loss to handle the extra dimension m introduced by our method.

---

[6]Gradient regularization was shown to be necessary in such methods [8], and also more recently in a general generative modeling context [31].

[7]There is however loss of information since the match is only *relative*. This may be a boon however, and allow the agent to focus on the relative importance of features, rather than their absolute magnitudes. Since the random prior vector is a near-orthogonal map of the input vector, much of the input's original structure is preserved in it. If the agent benefits from relative matching in the input space (e.g. coordination or locomotion task), then it should benefit from relative matching in the random prior embedding.

4.3.3 From Code to Bound: Deriving $\Lambda(\ell_{\mathrm{HLG}})$ via Implementation Analysis

We want to determine $\Lambda(\ell_{\mathrm{HLG}})$, the Lipschitz constant of the ℓ_{HLG} pairing loss. In particular, an insightful bound would reveal how the Lipschitz constant of ℓ_{HLG} **depends on its hyper-parameters**, especially σ and N, which together control the **label smoothing** capabilities of the loss. While Imani and White [32], who introduced this loss, derived a local Lipschitz continuity bound with respect to the *parameters*, we derive ours with respect to the *inputs*. Both their findings and ours point to the same insight: the gradients are well-behaved. The part of their bound that concerns the Lipschitz continuity with respect to the inputs is simply the absolute bin-wise difference between predicted probability and transformed target bin value. We go further than that stage, considering the worst-case scenario, and proceeding until the bound can only be expressed with the hyper-parameters of ℓ_{HLG}.

Based on our implementation of the ℓ_{HLG} loss—see SNIPPET 1 in APPENDIX C, we want to upper bound the Lipschitz constant of the loss *w.r.t.* its inputs. In the interest of space, we provide the intermediary results and their derivations in APPENDIX H. We first establish the theoretical framework by formalizing the elements involved in the snippet of the loss. We carry this out in DEF H.1. After establishing the groundwork, we present our core theoretical result, TH H.2, which expresses the Lipschitz constant of ℓ_{HLG} in terms of the maximal reachable probability mass $p_{\max}$. We then develop a lemma LEM H.3, in which we derive an estimate of $p_{\max}$, which ultimately enables us to express $\Lambda(\ell_{\mathrm{HLG}})$ with respect to the hyper-parameters of the loss *only*, in TH 4.2. As such, our series of theoretical results leads us to the insightful bound to we set out to derive at the start of this section.

Theorem 4.2 (Lipschitz continuity of ℓ_{HLG}). *The loss histogram loss "Gaussian type" ℓ_{HLG} is Λ-Lipschitz continuous with respect to the logits, with a Lipschitz constant that verifies the inequality:*

$$\Lambda \leq \sqrt{1 + \left(\frac{C}{\sigma}\right)^2} \tag{5}$$

where $C := \Delta s \sqrt{(N-1)/(2\pi)}$. Δs is the bin width (introduced in DEF H.1). Note, this result is subject to the approximation considerations from LEM H.3. Refer to APPENDIX H for greater details.

Discussion of guarantees and implications. Theorem TH 4.2 shows how the Lipschitz constant of the function $x \mapsto \ell_{\mathrm{HLG}}(x, t)$ depends on σ. As $\sigma \to +\infty$, $C/\sigma \to 0$, so the upper bound on Λ approaches 1. As $\sigma \to 0$ however, $C/\sigma \to +\infty$. This tells us that, when the Normal distribution is extremely narrow, the Lipschitz constant of ℓ_{HLG} can grow unbounded. This translates to high sensitivity and therefore poor stability. As such, TH 4.2 advises for the use of a σ value that is **high enough** with respect to the number of bins and the interval bounds a and b to prevent unsteadiness.

Code is publicly available at: `https://github.com/lionelblonde/ngt-pytorch`.

5 Experiments

We now evaluate the sample-efficiency and stability of NGT against a set of baseline methods across a suite of continuous control environments. We begin by describing the experimental setup, then present the baselines used for comparison. Finally, we report the results and discuss their implications.

All methods were re-implemented from a shared SAC-based actor-critic backbone, differing only in how the reward is computed or learned. APPENDIX L details the modifications made to DiffAIL [60], where we adapt the original reward implementation to ensure numerical stability. The general network architecture used across methods is shown in APPENDIX I. We share the hyperparameters in APPENDIX L. We compare NGT to baselines across environments with varying numbers of expert demonstrations (1, 4, and 11), subsampled at a rate of 20 with varying offsets, as in [28, 37, 7, 16]. Under that setting, 1 demonstration comprises 50 transitions (since they originally are composed of 1000 each). We use vectorized environments, with 4 parallel executors. When one step is carried out, we increment the counter by 4, reflecting the *true* number of interactions with *an* environment. Our experts are policies trained with SAC in the same environment as the agent, but using a different random seed. Each experiment is run with 4 random seeds. During evaluation, a new seed is sampled from the initial one given to the agent *at each episode reset*, ensuring that each evaluation episode uses a different environment instance. This setup **prevents the agent from memorizing trajectories and encourages genuine generalization toward expert behavior**. We tackle the Gymnasium continuous
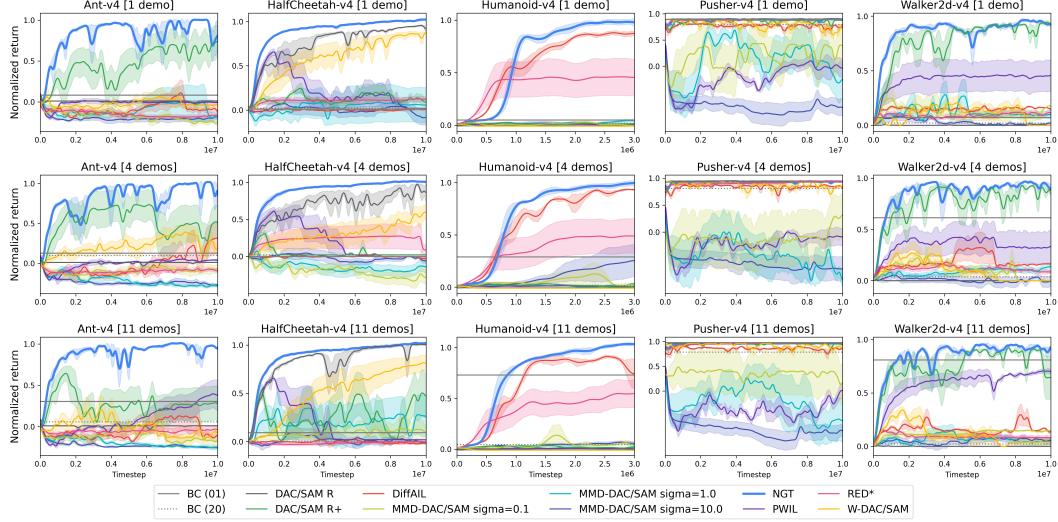
Figure 2: Performance comparison over various environments and numbers of demonstrations.

control suite [58], whose complexity culminates with `Humanoid-v4`. We report the dimensions of the state and action spaces in APPENDIX M.

As tensor software, we use PyTorch [45] and CUDA Graphs (APPENDIX K). CUDA Graphs enabled up to a 3x speedup for all algorithms; ≈ 5 hours of training time for a humanoid on GPU. Each method tested fits within the memory of an NVIDIA RTX 4090 card, except DiffAIL for which we suggest reducing the replay buffer capacity by 1M to fit.

We consider baselines that are either offline, or online off-policy. BC operates pure supervised learning on expert pairs (offline). We show two variants: BC with with the same subsampling as the other methods, and BC *without* any—we simply call the latter `BC(1)`. We find this adds perspective on **how data sparsity and scarcity impact the performance**. For example, `BC(1)` performs very well on `Humanoid-v4` with 11 demonstrations (11K pairs to train on). So, when expert data is abundant, BC is indeed a good option. Another method is PWIL [16] which iteratively solve a procedure aimed at minimizing the EMD in its *primal* form. As such, it *computes* a reward; it does not *learn* one. Next, we group DAC [37] and SAM [7] under a common framework. Both methods train their reward function using a JS-GAN discriminator. We refer to this combined baseline as `DAC/SAM` in the plots. We show two variants: `R+` uses $-log(1 - D)$ as reward ($\in \mathbb{R}_+$), and `R` uses $-log(1 - D) + log(D)$ ($\in \mathbb{R}$). `W-DAC/SAM` turns the JS-GAN discriminator into a WGAN critic [3], and `MMD-DAC/SAM` replaces the EMD-maximizing objective of the WGAN critic with an MMD divergence (RBF, $\sigma \in \{0.1, 1, 10\}$) [39, 64]. We replicate RED [61] by only using the left term of $L(\xi)$ in NGT. The method is denoted `RED*`, where the $*$ signifies that we apply an adaptive reward numerics scheme (APPENDIX J) instead of tuning a temperature parameter per environment like the original RED does. Finally, DiffAIL relies on a diffusion/de-noising task and uses the diffusion error in place of the discriminator output in a JS-GAN objective. Crucially, *only the reward model is diffusion-based*. Since the authors do not treat a `Humanoid` in the environment-specific configuration files of their codebase, we started our search from the hyper-parameters they used for `Ant`. Specifically, we use a gradient penalty coefficient of 0.1 for DiffAIL, and the recommended 10 for the other *dual* adversarial methods. Note, **NGT did not require a gradient penalty regularizer outside spectral normalization**, which is something DAC/SAM could not get away with, as show in [8]. We hypothesize that this effect stems from the greater numerical stability and smoother learning dynamics enabled by the potential function used in our reward learning design.

Unless stated otherwise, all reported **returns are normalized per task** such that a score of 0 corresponds to the performance of a random agent, and 1 to that of the expert. Returns below the random baseline then yield negative scores.
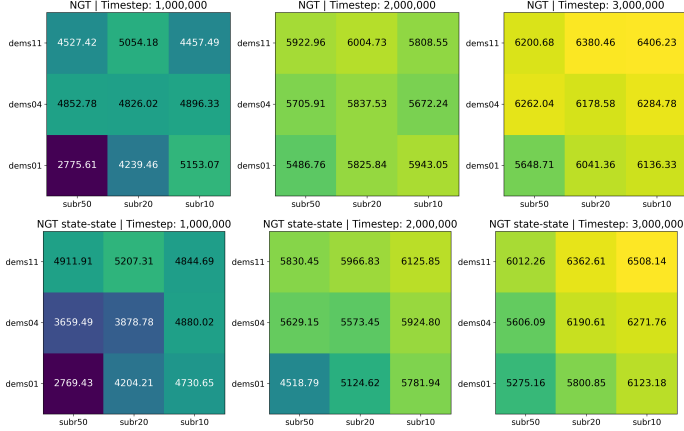
8

Figure 3: NGT's unnormalized performance across varying numbers of demonstrations and subsampling rates, in the *state-action* (first row) and *state-state* setting (second row), in `Humanoid-v4`.

We present the **main results** in FIGURE 2, with an aggregated view shown in FIGURE 1. In FIGURE 3, we further examine how NGT performs across finer-grained settings, varying both the number of demonstrations and the subsampling rate, in both the state-action and state-state scenarios. FIGURES 2 and 3 report results from 720 and 72 experiments, respectively.

Overall, FIGURES 1 and 2 shows that NGT achieves expert performance across the board and outperforms the baselines. DiffAIL shows strong performance on `Humanoid-v4`, seemingly leveraging the high representational power of its diffusion model. Yet, it struggles in most of the others. Deeper per-environment tuning might make DiffAIL perform better, but we did not carry out per-task tuning for any method. FIGURE 3 shows that NGT exhibits consistent and stable scaling—even in the state-state setting. The figures also show that optimizing an EMD is not the whole story, or at least that it is not easy to estimate an EMD properly, judging by the difference in results between NGT and WGAN. Unlike binary classification—which may become trivial early in training and require strong regularization like gradient penalization —the m-dimensional prior prediction task scales more gracefully with model capacity. The histogram loss ℓ_{HLG} has the ability to apply σ-controlled label smoothing. In particular, since the pairing loss appears *twice* in the reward loss, we have the option to use different σ's on each side. To emulate the typical JS-GAN trick of smoothing only the expert-side labels, we can use a higher σ value in the expert-side expectation of $L(\xi)$. Furthermore, we support the design choices made in NGT through a series of **ablation studies** presented in APPENDIX N, and extend our analysis to **extra environments** in APPENDIX O.

Finally, we report a comparison of baseline **speeds** in APPENDIX P.

6 Conclusion

In this work, we develop Noise-Guided Transport (NGT), a sample-efficient imitation learning method in the low-data regime, where only a handful of demonstrations are available. The reward learning objective of NGT builds on prediction from random priors, and optimizes a distance rooted in optimal transport theory. Moreover, by leveraging distributional losses, NGT succeeds in learning to reproduce humanoid gaits, with as few as 20 transitions, even when actions are unavailable. It outperforms all baselines, and does not require gradient penalization. An intriguing direction for future work is to investigate the applicability of this objective to general generative modeling tasks.

Beyond these technical contributions, we hope this work helps to re-spark interest in imitation learning under data-limited settings, enabling progress in applied domains such as **biorobotics and healthcare**, where demonstrations are extremely scarce and demand special care and considerations.

7   Reproducibility

All code, configuration files, and instructions for reproducing our experiments are publicly available at `https://github.com/lionelblonde/ngt-pytorch`. This enables the exact replication of all experiments reported in the paper. The code integrates all baselines into a unified framework with a common SAC backbone, optimizer, and evaluation pipeline, so that the only variation across methods is the reward mechanism. This ensures that performance differences are attributable to algorithmic design rather than implementation details, and allows for consistent, reproducible comparisons. Moreover, all proofs for the theoretical results are given in the appendix. Empirical and theoretical contributions can thus be independently verified.

References

[1] Pieter Abbeel and Andrew Y Ng. Apprenticeship Learning via Inverse Reinforcement Learning. In *International Conference on Machine Learning (ICML)*, 2004.

[2] Cem Anil, James Lucas, and Roger Grosse. Sorting Out Lipschitz Function Approximation. In *International Conference on Machine Learning (ICML)*, pages 291–301. PMLR, 2019.

[3] Martin Arjovsky, Soumith Chintala, and Léon Bottou. Wasserstein GAN. *arXiv [stat.ML]*, January 2017.

[4] Jimmy Lei Ba, Jamie Ryan Kiros, and Geoffrey E Hinton. Layer Normalization. *arXiv [stat.ML]*, July 2016.

[5] J Andrew Bagnell. An invitation to imitation. Technical report, Carnegie Mellon, Robotics Institute, Pittsburgh, 2015.

[6] Kevin Black, Noah Brown, Danny Driess, Adnan Esmail, Michael Equi, Chelsea Finn, Niccolo Fusai, Lachy Groom, Karol Hausman, Brian Ichter, Szymon Jakubczak, Tim Jones, Liyiming Ke, Sergey Levine, Adrian Li-Bell, Mohith Mothukuri, Suraj Nair, Karl Pertsch, Lucy Xiaoyang Shi, James Tanner, Quan Vuong, Anna Walling, Haohuan Wang, and Ury Zhilinsky. π_0: A vision-language-action flow model for general robot control. *arXiv [cs.LG]*, October 2024.

[7] Lionel Blondé and Alexandros Kalousis. Sample-Efficient Imitation Learning via Generative Adversarial Nets. In *International Conference on Artificial Intelligence and Statistics (AISTATS)*, 2019.

[8] Lionel Blondé, Pablo Strasser, and Alexandros Kalousis. Lipschitzness Is All You Need To Tame Off-policy Generative Adversarial Imitation Learning. *arXiv [cs.LG]*, June 2020.

[9] Yuri Burda, Harrison Edwards, Amos Storkey, and Oleg Klimov. Exploration by Random Network Distillation. *arXiv [cs.LG]*, October 2018.

[10] Jonathan D Chang, Dhruv Sreenivas, Yingbing Huang, Kianté Brantley, and Wen Sun. Adversarial Imitation Learning via Boosting. In *International Conference on Learning Representations (ICLR)*, 2024.

[11] Ting Chen, Simon Kornblith, Mohammad Norouzi, and Geoffrey Hinton. A Simple Framework for Contrastive Learning of Visual Representations. In *International Conference on Machine Learning (ICML)*, 2020.

[12] Cheng Chi, Siyuan Feng, Yilun Du, Zhenjia Xu, Eric Cousineau, Benjamin Burchfiel, and Shuran Song. Diffusion Policy: Visuomotor Policy Learning via Action Diffusion. *arXiv [cs.RO]*, March 2023.

[13] Paul Christiano, Jan Leike, Tom B Brown, Miljan Martic, Shane Legg, and Dario Amodei. Deep reinforcement learning from human preferences. In *Neural Information Processing Systems (NeurIPS)*, 2017.

[14] Kamil Ciosek, Vincent Fortuin, Ryota Tomioka, Katja Hofmann, and Richard Turner. Conservative Uncertainty Estimation By Fitting Prior Networks. In *International Conference on Learning Representations (ICLR)*, 2020.

[15] Robert H Crites and Andrew G Barto. An Actor/Critic Algorithm that is Equivalent to Q-Learning. In *Neural Information Processing Systems (NeurIPS)*, 1995.

[16] Robert Dadashi, Léonard Hussenot, Matthieu Geist, and Olivier Pietquin. Primal Wasserstein Imitation Learning. In *International Conference on Learning Representations (ICLR)*, 2021.

[17] Jesse Farebrother, Jordi Orbay, Quan Vuong, Adrien Ali Taïga, Yevgen Chebotar, Ted Xiao, Alex Irpan, Sergey Levine, Pablo Samuel Castro, Aleksandra Faust, Aviral Kumar, and Rishabh Agarwal. Stop Regressing: Training Value Functions via Classification for Scalable Deep RL. Technical report, DeepMind, March 2024.

[18] Chelsea Finn, Paul Christiano, Pieter Abbeel, and Sergey Levine. A Connection between Generative Adversarial Networks, Inverse Reinforcement Learning, and Energy-Based Models. *arXiv [cs.LG]*, November 2016.

[19] Nicolas Fournier and Arnaud Guillin. On the rate of convergence in Wasserstein distance of the empirical measure. *Probab. Theory Relat. Fields*, 162(3-4):707–738, August 2015.

[20] Seyed Kamyar Seyed Ghasemipour, Richard Zemel, and Shixiang Gu. A Divergence Minimization Perspective on Imitation Learning Methods. In *Conference on Robot Learning (CoRL)*, 2019.

[21] Ian Goodfellow, Jean Pouget-Abadie, Mehdi Mirza, Bing Xu, David Warde-Farley, Sherjil Ozair, Aaron Courville, and Yoshua Bengio. Generative Adversarial Nets. In *Neural Information Processing Systems (NIPS)*, 2014.

[22] Ishaan Gulrajani, Faruk Ahmed, Martin Arjovsky, Vincent Dumoulin, and Aaron Courville. Improved Training of Wasserstein GANs. In *Neural Information Processing Systems (NIPS)*, 2017.

[23] Tuomas Haarnoja, Aurick Zhou, Pieter Abbeel, and Sergey Levine. Soft Actor-Critic: Off-Policy Maximum Entropy Deep Reinforcement Learning with a Stochastic Actor. In *International Conference on Machine Learning (ICML)*, 2018.

[24] Danijar Hafner, Jurgis Pasukonis, Jimmy Ba, and Timothy Lillicrap. Mastering Diverse Domains through World Models. *arXiv [cs.AI]*, January 2023.

[25] Siddhant Haldar, Vaibhav Mathur, Denis Yarats, and Lerrel Pinto. Watch and Match: Supercharging Imitation with Regularized Optimal Transport. In *Conference on Robot Learning (CoRL)*, 2022.

[26] Nicklas Hansen, Hao Su, and Xiaolong Wang. TD-MPC2: Scalable, Robust World Models for Continuous Control. In *International Conference on Learning Representations (ICLR)*, 2024.

[27] Kaiming He, Xiangyu Zhang, Shaoqing Ren, and Jian Sun. Delving deep into rectifiers: Surpassing human-level performance on ImageNet classification. In *International Conference on Computer Vision (ICCV)*, pages 1026–1034, 2015.

[28] Jonathan Ho and Stefano Ermon. Generative Adversarial Imitation Learning. In *Neural Information Processing Systems (NIPS)*, 2016.

[29] Ming Hou, Brahim Chaib-draa, Chao Li, and Qibin Zhao. Generative Adversarial Positive-Unlabeled Learning. In *International Joint Conference on Artificial Intelligence (IJCAI)*, 2018.

[30] Wei Hu, Lechao Xiao, and Jeffrey Pennington. Provable Benefit of Orthogonal Initialization in Optimizing Deep Linear Networks. In *International Conference on Learning Representations (ICLR)*, 2020.

[31] Yiwen Huang, Aaron Gokaslan, Volodymyr Kuleshov, and James Tompkin. The GAN is dead; long live the GAN! A Modern GAN Baseline. In *Neural Information Processing Systems (NeurIPS)*, 2024.

[32] Ehsan Imani and Martha White. Improving Regression Performance with Distributional Losses. In *International Conference on Machine Learning (ICML)*, 2018.

[33] Jared Kaplan, Sam McCandlish, Tom Henighan, Tom B Brown, Benjamin Chess, Rewon Child, Scott Gray, Alec Radford, Jeffrey Wu, and Dario Amodei. Scaling Laws for Neural Language Models. Technical report, OpenAI, January 2020.

[34] Liyiming Ke, Matt Barnes, Wen Sun, Gilwoo Lee, Sanjiban Choudhury, and Siddhartha Srinivasa. Imitation Learning as f-Divergence Minimization. *arXiv [cs.LG]*, May 2019.

[35] Grigory Khromov and Sidak Pal Singh. Some Fundamental Aspects about Lipschitz Continuity of Neural Networks. In *International Conference on Learning Representations (ICLR)*, 2024.

[36] Diederik P Kingma and Jimmy Ba. Adam: A Method for Stochastic Optimization. *arXiv [cs.LG]*, December 2014.

[37] Ilya Kostrikov, Kumar Krishna Agrawal, Debidatta Dwibedi, Sergey Levine, and Jonathan Tompson. Discriminator-Actor-Critic: Addressing Sample Inefficiency and Reward Bias in Adversarial Imitation Learning. In *International Conference on Learning Representations (ICLR)*, 2019.

[38] Pablo Lemos, Adam Coogan, Yashar Hezaveh, and Laurence Perreault-Levasseur. Sampling-based accuracy testing of posterior estimators for general inference. In *International Conference on Machine Learning (ICML)*, 2023.

[39] Chun-Liang Li, Wei-Cheng Chang, Yu Cheng, Yiming Yang, and Barnabás Póczos. MMD GAN: Towards deeper understanding of moment matching network. *arXiv [cs.LG]*, May 2017.

[40] Long-Ji Lin. Self-improving reactive agents based on reinforcement learning, planning and teaching. *Mach. Learn.*, 8(3):293–321, May 1992.

[41] Colin McDiarmid. On the method of bounded differences. *Surveys in combinatorics*, 141(1): 148–188, 1989.

[42] Takeru Miyato, Toshiki Kataoka, Masanori Koyama, and Yuichi Yoshida. Spectral Normalization for Generative Adversarial Networks. In *International Conference on Learning Representations (ICLR)*, 2018.

[43] Alexander Nikulin, Vladislav Kurenkov, Denis Tarasov, and Sergey Kolesnikov. Anti-exploration by Random Network Distillation. In *International Conference on Machine Learning (ICML)*, January 2023.

[44] Ian Osband, Benjamin Van Roy, and Zheng Wen. Generalization and Exploration via Randomized Value Functions. *arXiv [stat.ML]*, February 2014.

[45] Adam Paszke, Sam Gross, Francisco Massa, Adam Lerer, James Bradbury, Gregory Chanan, Trevor Killeen, Zeming Lin, Natalia Gimelshein, Luca Antiga, Alban Desmaison, Andreas Kopf, Edward Yang, Zachary DeVito, Martin Raison, Alykhan Tejani, Sasank Chilamkurthy, Benoit Steiner, Lu Fang, Junjie Bai, and Soumith Chintala. PyTorch: An Imperative Style, High-Performance Deep Learning Library. In *Neural Information Processing Systems (NeurIPS)*, 2019.

[46] Ethan Perez, Florian Strub, Harm de Vries, Vincent Dumoulin, and Aaron Courville. FiLM: Visual Reasoning with a General Conditioning Layer. In *Conference on Artificial Intelligence (AAAI)*, 2018.

[47] Dean Pomerleau. ALVINN: An Autonomous Land Vehicle in a Neural Network. In *Neural Information Processing Systems (NIPS)*, pages 305–313, 1989.

[48] Rafael Rafailov, Archit Sharma, Eric Mitchell, Stefano Ermon, Christopher D Manning, and Chelsea Finn. Direct Preference Optimization: Your Language Model is Secretly a Reward Model. In *Neural Information Processing Systems (NeurIPS)*, 2023.

[49] João A Cândido Ramos, Lionel Blondé, Naoya Takeishi, and Alexandros Kalousis. Mimicking better by matching the approximate action distribution. In *International Conference on Machine Learning (ICML)*, 2024.

[50] Alexandre Ramé, Nino Vieillard, Léonard Hussenot, Robert Dadashi, Geoffrey Cideron, Olivier Bachem, and Johan Ferret. WARM: On the Benefits of Weight Averaged Reward Models. Technical report, DeepMind, January 2024.

[51] Shideh Rezaeifar, Robert Dadashi, Nino Vieillard, Léonard Hussenot, Olivier Bachem, Olivier Pietquin, and Matthieu Geist. Offline Reinforcement Learning as anti-exploration. In *Conference on Artificial Intelligence (AAAI)*, 2022.

[52] Stéphane Ross and J Andrew Bagnell. Efficient Reductions for Imitation Learning. In *International Conference on Artificial Intelligence and Statistics (AISTATS)*, 2010.

[53] Andrew M Saxe, James L McClelland, and Surya Ganguli. Exact solutions to the nonlinear dynamics of learning in deep linear neural networks. *arXiv [cs.NE]*, December 2013.

[54] Hao Sun. Supervised Fine-Tuning as Inverse Reinforcement Learning. *arXiv [cs.LG]*, March 2024.

[55] Richard S Sutton and Andrew G Barto. *Reinforcement Learning: An Introduction (second edition)*. MIT Press, 2018.

[56] Christian Szegedy, Vincent Vanhoucke, Sergey Ioffe, Jonathon Shlens, and Zbigniew Wojna. Rethinking the Inception Architecture for Computer Vision. In *Conference on Computer Vision and Pattern Recognition (CVPR)*, 2016.

[57] Yuval Tassa, Yotam Doron, Alistair Muldal, Tom Erez, Yazhe Li, Diego de Las Casas, David Budden, Abbas Abdolmaleki, Josh Merel, Andrew Lefrancq, Timothy Lillicrap, and Martin Riedmiller. DeepMind Control Suite. *arXiv [cs.AI]*, January 2018.

[58] Mark Towers, Ariel Kwiatkowski, Jordan Terry, John U Balis, Gianluca De Cola, Tristan Deleu, Manuel Goulão, Andreas Kallinteris, Markus Krimmel, Arjun KG, et al. Gymnasium: A standard interface for reinforcement learning environments. *arXiv preprint arXiv:2407.17032*, 2024.

[59] Cedric Villani. *Optimal Transport: Old and New*. Grundlehren der mathematischen Wissenschaften. Springer, Berlin, Germany, December 2009.

[60] Bingzheng Wang, Guoqiang Wu, Teng Pang, Yan Zhang, and Yilong Yin. DiffAIL: Diffusion Adversarial Imitation Learning. In *Conference on Artificial Intelligence (AAAI)*, December 2023.

[61] Ruohan Wang, Carlo Ciliberto, Pierluigi Amadori, and Yiannis Demiris. Random Expert Distillation: Imitation Learning via Expert Policy Support Estimation. In *International Conference on Machine Learning (ICML)*, 2019.

[62] Jonathan Weed and Francis Bach. Sharp asymptotic and finite-sample rates of convergence of empirical measures in Wasserstein distance. *Bernoulli (Andover.)*, 25(4A):2620–2648, November 2019.

[63] Markus Wulfmeier, Michael Bloesch, Nino Vieillard, Arun Ahuja, Jorg Bornschein, Sandy Huang, Artem Sokolov, Matt Barnes, Guillaume Desjardins, Alex Bewley, Sarah Maria Elisabeth Bechtle, Jost Tobias Springenberg, Nikola Momchev, Olivier Bachem, Matthieu Geist, and Martin Riedmiller. Imitating language via scalable inverse reinforcement learning. *arXiv [cs.LG]*, September 2024.

[64] Huang Xiao, Michael Herman, Joerg Wagner, Sebastian Ziesche, Jalal Etesami, and Thai Hong Linh. Wasserstein Adversarial Imitation Learning. *arXiv [cs.LG]*, June 2019.

[65] Zhuangdi Zhu, Kaixiang Lin, Bo Dai, and Jiayu Zhou. Off-policy imitation learning from observations. In *Neural Information Processing Systems (NeurIPS)*, 2020.

[66] Brian D Ziebart, Andrew L Maas, J Andrew Bagnell, and Anind K Dey. Maximum Entropy Inverse Reinforcement Learning. In *AAAI Conference on Artificial Intelligence*, pages 1433–1438, 2008.

A Algorithm

In ALGO 1, the learned reward structure laid out in EQ **??** takes the triplet (s_t, a_t, s_{t+1}) as input to signify that depending on the setting, the reward could be trained to use any of the following input combinations: (s_t, a_t), (s_t, s_{t+1}), or s_t.

Algorithm 1 Noise-Guided Transport (NGT) Algorithm (as presented in this work)

1: Initialize parameters of policy network π_θ, Q-networks Q_{ω_1}, Q_{ω_2}, target Q-network parameters $\bar{\omega}_1 \leftarrow \omega_1, \bar{\omega}_2 \leftarrow \omega_2$, and reward model r_ξ
2: Initialize temperature parameter α and target entropy $\mathcal{H}$
3: Initialize replay buffer $\mathcal{D}$ and expert demonstration dataset $\mathcal{E}$
4: **for** each iteration **do**
5:     **for** each environment step **do**
6:         Sample action $a_t \sim \pi_\theta(a_t|s_t)$
7:         Execute a_t in environment, observe s_{t+1}
8:         Store (s_t, a_t, s_{t+1}) in $\mathcal{D}$
9:         `// not storing rewards`
10:     **end for**
11:     **for** each gradient step **do**
12:         `// Update reward model`
13:         Sample a minibatch of transitions (s_t, a_t, s_{t+1}) $\mathcal{B}_\mathcal{E}$ from expert dataset $\mathcal{E}$
14:         Sample a minibatch of transitions (s_t, a_t, s_{t+1}) $\mathcal{B}_\mathcal{D}$ from replay buffer $\mathcal{D}$
15:         Update reward model parameters ξ by minimizing:

$$L(\xi) = \frac{1}{|\mathcal{B}_\mathcal{E}|} \sum_{t \in \mathcal{B}_\mathcal{E}} h_\xi(s_t, a_t, s_{t+1}) - \frac{1}{|\mathcal{B}_\mathcal{D}|} \sum_{t \in \mathcal{B}_\mathcal{D}} h_\xi(s_t, a_t, s_{t+1})$$

16:         `// Update actor-critic`
17:         Sample a minibatch of transitions (s_t, a_t, s_{t+1}) from $\mathcal{D}$
18:         Compute target Q-value using reward model r_ξ:

$$y_t = r_\xi(s_t, a_t, s_{t+1}) + \gamma \mathbb{E}_{a_{t+1} \sim \pi_\theta} \left[\min_{i=1,2} Q_{\bar{\omega}_i}(s_{t+1}, a_{t+1}) - \alpha \log \pi_\theta(a_{t+1}|s_{t+1}) \right]$$

19:         Update Q-function parameters ω_i by minimizing:

$$L(\omega_i) = \frac{1}{|\mathcal{B}_\mathcal{D}|} \sum_{t \in \mathcal{B}_\mathcal{D}} (Q_{\omega_i}(s_t, a_t) - y_t)^2 \quad \text{for } i = 1, 2$$

20:         Update policy parameters θ by minimizing:

$$L(\theta) = \frac{1}{|\mathcal{B}_\mathcal{D}|} \sum_{t \in \mathcal{B}_\mathcal{D}} \mathbb{E}_{a_t \sim \pi_\theta} \left[\alpha \log \pi_\theta(a_t|s_t) - \min_{i=1,2} Q_{\omega_i}(s_t, a_t) \right]$$

21:         Adjust temperature α (optional) by minimizing:

$$L(\alpha) = -\frac{1}{|\mathcal{B}_\mathcal{D}|} \sum_{t \in \mathcal{B}_\mathcal{D}} \alpha \left(\log \pi_\theta(a_t|s_t) + \mathcal{H} \right)$$

22:         Update target Q-network parameters:

$$\bar{\omega}_i \leftarrow \tau \omega_i + (1 - \tau)\bar{\omega}_i \quad \text{for } i = 1, 2$$

23:     **end for**
24: **end for**

B   HL-Gaussian Loss: Mechanism and How We Extend It

In essence, ℓ_{HLG} maps the scalar target onto N bins (spread evenly across $[a, b]$) using a transformation that assigns the highest probability mass to the bin containing the scalar, while distributing the remaining mass to neighboring bins in the shape of a bell curve. This redistribution of mass to adjacent locations is akin to target smoothing. The model being trained with this loss predicts one value per bin, i.e. a N-dimensional output. Those logits are transformed into probabilities with a softmax layer. The two vectors of size N are then compared using cross-entropy. To compare f_ξ to $f_\xi^\dagger$, we therefore introduce *asymmetry* in their architecture. The random priors are still in $\mathbb{R}^m$, but the predictor returns an embedding in $\mathbb{R}^{m \times N}$ (column vector). It is then rearranged into a $N \times m$ matrix ($\in \mathcal{M}_{m,N}(\mathbb{R})$). After softmax-ing row-wise, each now of this matrix is a vector whose N elements are interpreted as predicted probabilities over bins. On the target side, the m scalar random priors returned by $f_\xi^\dagger$ are each transformed into a probability vector spanning N bins. In effect, we now have a $\mathcal{M}_{m,N}(\mathbb{R})$ matrix from $f_\xi^\dagger$ and from $f_\xi^\dagger$. Finally, the matrices are compared row-wise using N-bin cross-entropy. Our implementation of the ℓ_{HLG} loss is given in SNIPPET 1, in APPENDIX C,

C   HL-Gaussian Loss: Code Snippet

In this section, we provide a PyTorch [45] code snippet of our augmented implementation of the HL-Gaussian loss [32]. Our code builds on the reference snippet shared in the appendix of Farebrother et al. [17], with several modifications. One change that significantly improved numerical stability was the addition of a small constant $\epsilon = 10^{-6}$ to the denominator in the `transform_to_probs` function, as shown in SNIPPET 1. Matrix reshaping into $\mathcal{M}_{m,N}(\mathbb{R})$ is carried out using the `einops` library.

Listing 1: HL-Gaussian loss

```python
from einops import rearrange
import torch
from torch import nn
from torch.nn import functional as ff


class HLGaussLoss(nn.Module):

    def __init__(self,
                 *,
                 min_value: float,
                 max_value: float,
                 num_bins: int,
                 sigma: float,
                 device: torch.device,
                 reduction: str = "none"):
        super().__init__()
        self.min_value = min_value
        self.max_value = max_value
        self.num_bins = num_bins
        self.sigma = sigma
        self.device = device
        self.reduction = reduction
        self.support = torch.linspace(
            min_value, max_value, num_bins + 1, dtype=torch.float, device=self.device)
        self.sqrt_of_two = torch.sqrt(torch.tensor(2.0, device=self.device))

    def forward(self, logits: torch.Tensor, target: torch.Tensor) -> torch.Tensor:
        logits = rearrange(logits, "b (c d)-> b c d", c=self.num_bins)
        target_probs = self.transform_to_probs(target)
        target_probs = rearrange(target_probs, "b d c-> b c d", c=self.num_bins)
        return ff.cross_entropy(logits, target_probs, reduction=self.reduction)

    def transform_to_probs(self, target: torch.Tensor) -> torch.Tensor:
        operand1 = self.support - target.unsqueeze(-1)
        operand2 = self.sqrt_of_two * self.sigma
        operand = operand1 / operand2
        cdf_evals = torch.special.erf(operand)
        z = cdf_evals[..., -1] - cdf_evals[..., 0]
        bin_probs = cdf_evals[..., 1:] - cdf_evals[..., :-1]
        return bin_probs / (z + 1e-6).unsqueeze(-1)

    def transform_from_probs(self, probs: torch.Tensor) -> torch.Tensor:
        centers = (self.support[:-1] + self.support[1:]) / 2
        return torch.sum(probs * centers, dim=-1)
```

15

D   Related Works (Expansion)

In this section, we expand upon the related work discussed in SECTION 2.

The structure of the loss we train our reward with, $\ell(f(x), f^\dagger(x))$, echoes the loss used for contrastive learning in self-supervised learning, $\ell(f(x), f(y))$ (*e.g.*, in SimCLR [11]). However, unlike contrastive learning, where y represents an augmented or semantically similar version of x, our formulation leverages $f^\dagger(x)$ as a prior/reference signal.

Concentration bounds in optimal transport (OT) provide guarantees on the convergence rate of empirical measures in Wasserstein distance (also called earth-move distance, EMD). [19] establishes explicit bounds on the Wasserstein distance, with rates that depend on the dimensionality of the space. Their results are particularly sharp in the one-dimensional case, such as traditional EMD. [59] serves as a comprehensive reference for OT theory, including Wasserstein concentration bounds. While Villani does not focus specifically on empirical concentration inequalities, key theoretical tools such as the Lipschitz constant and McDiarmid's inequality appear in derivations, like in ours. More recently, [62] provides a detailed analysis of finite-sample convergence rates, refining previous results and offering insights into high-dimensional settings. These add perspective to the concentration guarantees we derived in this work.

The influence of the Lipschitz constant on the reward function has been investigated in depth in [8]. The authors argue, using DAC [37] and SAM [7] as baselines, that gradient penalization [22] is necessary for learning in the off-policy setting, as spectral normalization [42] alone proves insufficient. In contrast, NGT (this work) succeeds with *only* spectral normalization. How to enforce Lipschitz-continuity in neural networks and how it impact their performance has also been tackled in [35]. Earlier in SECTION 4, we made a connection between RED [61] and one-class classification (positive-unlabeled, PU learning) as each posits only positive signal is available. PU learning was used in adversarial IL in [29] but resulted in subpar performance [8].

DreamerV3 [24] and TD-MPC2 [26] are other works that incorporate classification losses for value learning in RL, though not as their primary focus. In contrast, Farebrother et al. [17] explicitly centers on this idea, arguing that using classification losses for value learning enables RL to benefit from scale. Our findings support and extend their observations, in that we show that classification losses can also play a crucial role in reward learning, in an imitation learning context.

Reinforcement learning from human feedback (RLHF, [13]) has seen a monumental resurgence in recent years with the rise of conversational agents built from large language models (LLMs). RLHF is used in LLM post-training to align the agent with human incentives through a reward model. **Modern RLHF techniques align with our reward learning logic**: perform gradient descent on preferred behaviors and gradient ascent on undesired ones, **as in Direct Preference Optimization (DPO)** [48]. At the intersection of reward Lipschitz continuity and LLMs, WARM [50] highlights the critical role of strict reward regularity in ensuring the effectiveness of a reward model for LLM post-training. Their findings closely align with those of [8], which we previously discussed. Finally, a recent trend in the field views RLHF through the lens of inverse reinforcement learning (IRL), framing the reward model as an implicit representation of human preferences [63, 54]. **"RLHF as *adversarial* IRL" may soon emerge as a key direction in the field.**

Outside the scope of RL, Lemos et al. [38] created a technique based on random points to test the accuracy of posterior estimators. The technique is intended for evaluation rather than model training.

E   WGAN

In the WGAN [3] formulation, the potential function corresponds directly to the critic, and the generator is trained by gradient descent on the learned potential. By contrast, we train our actor-critic architecture via policy gradient, with a reward constructed from the learned potential h_ξ. Although both NGT and WGAN optimize an EMD, they rely on fundamentally different potential functions. Crucially, the behavior of these potentials can significantly affect learning dynamics and training stability, as demonstrated by our experimental results in SECTION 5, where the `W-DAC/SAM` baseline implements the WGAN potential. Notably, while the WGAN potential (i.e. the critic) takes value in $\mathbb{R}$, our potential h_ξ returns values in $\mathbb{R}_+$. What's more, while the WGAN critic is unconstrained

over $\mathbb{R}$, the values returned by our predictor network f_ξ are **implicitly anchored** by those of the prior network $f_\xi^\dagger$, which prevents h_ξ from attaining excessively large values in $L(\xi)$.

F Concentration of Empirical Objective: Theoretical Results and Proofs

The loss $L(\xi)$ derived in SECTION 4.1 to learn a robust reward signal is defined in EQ 2 as:

$$L(\xi) = \mathbb{E}_{x \sim P_{\text{expert}}}\big[h_\xi(x)\big] - \mathbb{E}_{x \sim P_{\text{agent}}}\big[h_\xi(x)\big]$$

where h_ξ is 1-Lipschitz *w.r.t.* a ground metric over the input space $\mathbb{X}$: $d(x, x')$, $\forall x, x' \in \mathbb{X}$. To support the reliability of this objective, **we set out to derive a concentration bound for its empirical estimate** $\hat{L}(\xi)$, computed from finite samples drawn from P_{expert} and P_{agent}. The diameter, for the input space $\mathbb{X}$ and ground metric d, is defined as $\operatorname{diam}(\mathbb{X}) := \sup_{x,x' \in \mathbb{X}} d(x, x')$. In what follows, We omit the "ξ" subscripts to lighten the notations ($h_\xi \to h$). Also, we consider the h functions that are Λ-Lipschitz: $h \in H^\Lambda$ ($H_\xi^\Lambda \to H^\Lambda$). We treat the case $\Lambda = 1$ in a corollary. Finally: $L(\xi) \to L$.

Assumption F.1. $\Lambda > 0$ and $\operatorname{diam}(\mathbb{X}) < +\infty$.

Theorem F.2 (Concentration bound for the reward loss). *Let* $X^e = \{x_1^e, \ldots, x_n^e\}$ *and* $X^a = \{x_1^a, \ldots, x_n^a\}$ *be sets of* n *independent samples drawn from* P_{expert} *and* P_{agent}. *Let* $h \in H_\Lambda$, *and let the empirical loss* $\hat{L}$ *be defined as:*

$$\hat{L} := \frac{1}{n} \sum_{i=1}^n h(x_i^e) - \frac{1}{n} \sum_{j=1}^n h(x_j^a) \tag{6}$$

*Then, the **deviation** of the empirical loss* $\hat{L}$ *(EQ 6) from its expected value* L *(EQ 2) verifies:*

$$\mathbb{P}\big(|\hat{L} - L| \geq \epsilon\big) \leq \exp\left(-\frac{\epsilon^2 n}{\Lambda^2 \operatorname{diam}(\mathbb{X})^2}\right) \tag{7}$$

The proof of TH F.2 relies on McDiarmid's method of bounded differences [41].

It proceeds as follows.

Proof. First, we conduct a sensitivity analysis of $\hat{L}$ by evaluating the **maximum change** in $\hat{L}$ when a single sample is substituted. Starting with the first term of $\hat{L}$, we see that a replacement $x_i^e \in X^e \to x_i^{e'}$, without loss of generality causes the change:

$$\left|\frac{h(x_i^e)}{n} - \frac{h(x_i^{e'})}{n}\right| = \frac{1}{n}\left|h(x_i^e) - h(x_i^{e'})\right| \tag{8}$$

Since this applies for any replacement in the first term of $\hat{L}$, we can try to upper bound the term above with a bound that does not depend on the indices of the samples, and that entity would then *bound all the differences* in the term.

$$\frac{1}{n}\left|h(x_i^e) - h(x_i^{e'})\right| \leq \frac{\Lambda}{n} d(x_i^e, x_i^{e'}) \leq \frac{\Lambda}{n} \operatorname{diam}(\mathbb{X}) \tag{9}$$

The first transition is due to h being Λ-Lipschitz continuous by assumption. The second applies the definition of diameter. By symmetry, the sensitivity is the same for every replacement in the second term of $\hat{L}$. Due to all the differences being bounded, we can use McDiarmid's inequality [41]. To compute the bound, we need to compute the sum of squares of the bounds of the individual changes. Since there are $2n$ replacements and that we upper-bounded every replacement by an index-independent value $(\Lambda/n) \operatorname{diam}(\mathbb{X})$, the total sensitivity to insert in McDiarmid's bound is:

$$S := 2n\left(\frac{\Lambda}{n} \operatorname{diam}(\mathbb{X})\right)^2 = 2\frac{\Lambda^2}{n} \operatorname{diam}(\mathbb{X})^2 \tag{10}$$

We conclude by using the inequality with the calculated S:

$$\mathbb{P}\big(|\hat{L} - L| \geq \epsilon\big) \leq \exp\left(-\frac{2\epsilon^2}{S}\right) \tag{11}$$

The reduction of the operand yields the result in TH F.2. □

A PAC-style bound (probably approximately correct) can easily be derived from TH F.2 by equaling the bound to a δ and reducing. We can also derive a **corollary** for the case "$h \in H^1$" $\Lambda = 1$.

Corollary F.3 (For $h \in H^1$).

$$\mathbb{P}\big(|\hat{L} - L| \geq \epsilon\big) \leq \exp\left(- \frac{\epsilon^2 n}{\operatorname{diam}(\mathbb{X})^2} \right) \tag{12}$$

The proof is immediate from TH F.2 by setting $\Lambda = 1$.

G Potential Function Lipschitz Continuity: Proof

We here provide a proof for the theorem TH 4.1, presented in SECTION 4.3 without proof.

This theorem characterizes the Lipschitz constant of the potential function h_ξ in terms of the Lipschitz constants of the individual functions that composes it: f_ξ, $f_\xi^\dagger$, and ℓ.

Proof. Let $\Lambda(\cdot)$ denote the Lipschitz constant of a given function. We aim to bound the Lipschitz constant of the composite function h_ξ. To do so, we derive an upper bound on the deviation of h_ξ in terms of its constituent functions. By the properties of Lipschitz continuity under composition:

$$\begin{aligned}
\big|h_\xi(x_1) - h_\xi(x_2)\big| &= \big|\ell\big(f_\xi(x_1), f_\xi^\dagger(x_1)\big) - \ell\big(f_\xi(x_2), f_\xi^\dagger(x_2)\big)\big| \\
&\leq \Lambda(\ell)\left(\|f_\xi(x_1) - f_\xi(x_2)\| + \|f_\xi^\dagger(x_1) - f_\xi^\dagger(x_2)\| \right) \\
&\leq \Lambda(\ell)\left(\Lambda(f_\xi)\, d(x_1, x_2) + \Lambda(f_\xi^\dagger)\, d(x_1, x_2) \right) \\
&= \Lambda(\ell)\big(\Lambda(f_\xi) + \Lambda(f_\xi^\dagger)\big)\, d(x_1, x_2)
\end{aligned} \tag{13}$$

$\forall x_1, x_2 \in \mathbb{X}$. Therefore, h_ξ is Lipschitz continuous with constant:

$$\Lambda(\ell)\big(\Lambda(f_\xi) + \Lambda(f_\xi^\dagger)\big) \tag{14}$$

with respect to the ground metric d over $\mathbb{X}$ with, $\forall x_1, x_2 \in \mathbb{X}$. $\qquad\square$

H HL-Gaussian Loss Lipschitz Continuity: Theoretical Results and Proofs

In this appendix, we present theoretical results and corresponding proofs demonstrating and characterizing the Lipschitz continuity of the HL-Gaussian loss function [32], introduced in SECTION 4.3.2.

Definition H.1 (Groundwork). Let $\{s_0, \ldots, s_N\}$ be a partition of the interval $[a, b]$ into N bins. As such, $s_0 = a$, $s_N = b$, and each bin has width $\Delta s := s_{i+1} - s_i$, $\forall i \in [0, N-1] \cap \mathbb{N}$. The general definition of probability for bin i, under the Normal distribution, is, $\forall t \in [a, b]$:

$$p_i(t) := \frac{\Phi_0\big(\frac{s_{i+1}-t}{\sigma}\big) - \Phi_0\big(\frac{s_i-t}{\sigma}\big)}{\Phi_0\big(\frac{b-t}{\sigma}\big) - \Phi_0\big(\frac{a-t}{\sigma}\big)} \tag{15}$$

where Φ_0 is the CDF of the standard normal distribution. The denominator ensures that if there were probability mass of the t-centered Gaussian to be put outside $[a, b]$ (then *truncated*), the bins would be rebalanced by being uniformly attributed the extra mass needed for the p_i's to sum up to 1. Φ_0 can be expressed with the *special function* erf. Hence:

$$p_i(t) = \frac{\operatorname{erf}\big(\frac{s_{i+1}-t}{\sqrt{2}\sigma}\big) - \operatorname{erf}\big(\frac{s_i-t}{\sqrt{2}\sigma}\big)}{\operatorname{erf}\big(\frac{b-t}{\sqrt{2}\sigma}\big) - \operatorname{erf}\big(\frac{a-t}{\sqrt{2}\sigma}\big)} \tag{16}$$

which is how the *target transformation* is operated for a scalar $t \in [a, b]$ in the code snippet CODE 1 in APPENDIX C.

Let $\tilde{x} := (x_0, \ldots, x_{N_1}) \in \mathbb{R}^N$ be a vector of *logits* (typically the output of neural net). Following, CODE 1 in APPENDIX C, we go from *predicted logits* to *predicted probabilities* with a **softmax** over

the $\mathbb{R}^N$ vector (also summing up to one by construction). The predicted distribution is denoted by q. The per-bin probability mass is:

$$q_i(\tilde{x}) := \frac{\exp(x_i)}{\sum_{j=0}^{N-1} \exp(x_j)} \tag{17}$$

$\forall i \in [0, N-1] \cap \mathbb{N}$. Finally, we define ℓ_{HLG} as the **cross-entropy** between the transformed target distribution $p(t)$ and the predicted distribution $q(\tilde{x})$. It is the bin-wise sum:

$$\ell_{\mathrm{HLG}}(\tilde{x}, t) := - \sum_{0}^{N-1} p_i(t) \log(q_i(\tilde{x})) \tag{18}$$

$\forall i \in [0, N-1] \cap \mathbb{N}$ and $\forall t \in [a, b]$.

Theorem H.2 (Lipschitz constant of ℓ_{HLG} ($p_{\max}$ version)). *For any vector of logits over bins $\tilde{x} \in \mathbb{R}^N$, and $\forall t \in [a, b]$, the loss ℓ_{HLG} is Λ-Lipschitz continuous w.r.t. $\tilde{x}$, with:*

$$\Lambda \leq \sqrt{1 + (N-1)p_{\max}^2} \tag{19}$$

where $p_{\max}$ is the maximal probability mass reachable by $p(t)$ on a bin of its support $[a, b]$. It is achieved on the bin k where the t value falls in ($p_k(t) = p_{\max}$), and upper bounds the mass of any other bin: $\forall i \neq k, p_i(t) \leq p_{\max}$.

Proof. Starting from a known result about the gradient of the cross-entropy over discrete vectors with softmax, we can write the partial derivative of ℓ_{HLG} w.r.t. x_j, which is:

$$\frac{\partial \ell_{\mathrm{HLG}}}{\partial x_j} = q_j(\tilde{x}) - p_j(t) \tag{20}$$

Hence:

$$\nabla_{\tilde{x}} \ell_{\mathrm{HLG}}(\tilde{x}, t) = \big(q_0(\tilde{x}) - p_0(t), \ldots, q_{N-1}(\tilde{x}) - p_{N-1}(t)\big) \tag{21}$$

The Lipschitz constant Λ measures how large the gradient can get across all possible $\tilde{x} \in \mathbb{R}^N$ and $t \in [a, b]$, *i.e.*:

$$\Lambda = \sup_{\tilde{x}, t} \|\nabla_{\tilde{x}} \ell_{\mathrm{HLG}}(\tilde{x}, t)\|_2 = \sup_{\tilde{x}, t} \|q(\tilde{x}) - p(t)\|_2 \tag{22}$$

In order to find an upper bound on Λ, consider the *worst-case* scenario: when the distributions differ the most. The predicted distribution at $\tilde{x}$, $q(\tilde{x})$, is a one-hot vector, without loss of generality with $q_j = 1$ and $q_i = 0$ for any $i \neq j$. The transformed target distribution at t, $p(t)$, has maximum probability mass in a bin k, such that $p_k(t) = p_{\max}$. In the worst case, $j \neq k$.

We square the norm above, under this worst-case mismatch:

$$\|q(\tilde{x}) - p(t)\|_2^2 = \big(1 - p_j(t)\big)^2 + \sum_{i \neq j} \big(0 - p_i(t)\big)^2 \tag{23}$$

Since in this imagined scenario, $j \neq k$, k is in the second term. We therefore upper bound each individual term of the sum by the term that has the highest value: the k-th one.

$$\sum_{i \neq j} p_i(t)^2 \leq (N-1)p_k(t)^2 = (N-1)p_{\max}^2 \tag{24}$$

Because $j \neq k$, all we can do is upper bound the first term $(1 - p_j(t))^2$ by 1. This concludes with the final result. $\qquad\square$

Lemma H.3 (Maximum probability mass $p_{\max}$). *The maximum value $p(t)$ can take on a bin, $p_{\max}$, verifies:*

$$p_{\max} \approx \frac{\Delta s}{\sigma \sqrt{2\pi}} \tag{25}$$

This approximation tends toward an equality as (1) the bin width Δs gets smaller w.r.t. σ ($\Delta s \ll \sigma$), and as (2) the interval $[a, b]$ in which t is defined covers most of the Gaussian's probability mass (e.g. $[a, b] \supset [t - 3\sigma, t + 3\sigma]$).

Proof. $p_{\max}$ denotes the maximum probability mass a bin takes. It is taken by $p(t)$ at the bin t falls in. Say it is bin k, without loss of generality. The PDF of the t-centered Normal $\mathcal{N}(t, \sigma)$ takes value $1/(\sigma\sqrt{2\pi})$ at t. If we assume that the Gaussian is approximately uniform over the bin containing t—bin k—we can approximate the numerator of the target transformation $p_i(t)$ (as laid out in DEF H.1) with the *area of the rectangle*:

$$p_{\max} = p_k(t) \approx \frac{\Delta s / (\sigma\sqrt{2\pi})}{\Phi_0\left(\frac{b-t}{\sigma}\right) - \Phi_0\left(\frac{a-t}{\sigma}\right)} \tag{26}$$

The approximation of the **numerator** by the area of a rectangle becomes increasingly valid (closer to equality) as the bin width decreases *w.r.t.* the statistic σ. In addition, the normalization factor in the **denominator** approaches 1 as the interval $[a, b]$ covers the space where the Gaussian centered at t would put probability mass. A good coverage would be ensured if $[t - 3\sigma, t + 3\sigma] \subset [a, b]$. $\qquad\square$

We now conclude the chain of theoretical results and proofs with TH 4.2, in the main text. The proof of TH 4.2 is straightforward, following directly from substituting the result of LEM H.3 into TH H.2.

I Network Architecture

The actor, critic, and reward networks all have two hidden layers of width 256 units. The actor and critic use ReLU activations, while the reward network *all* use LeakyReLU activations with leak 0.05. We did *not* use layer normalization [4] in *any* network, and used orthogonal initialization [53, 30] in every network. We used spectral normalization [42] for every layer of the reward network.

We tried the asymmetric architecture proposed in [43], where predictor and prior networks have different architectures involving new ways of extracting features from state and action in a continuous control context—the context we consider in this work. Among the techniques in use are bilinear layers and FiLM [46]. The authors seem the get benefits from the proposed changes in feature engineering for offline RL. We however have not seen any benefit from this architecture. Besides, it has a significant toll on computational complexity. **In this work, we have show that it is possible to use a signal learned from random priors to solve tasks in continuous control**, which is what their architecture was claimed to unlock.

J Reward Numerics

Since different losses ℓ lead to different scales, it can be hard to determine the effectiveness of a loss design simply because the scale and shift of the resulting rewards might disagree with the agent. In order to have a controlled environment in which ℓ choices can be compared with minimal confounding factors, we adopt a simple scaling and shifting scheme to the designed reward. It could rely on the mean and standard deviation of the reward over the mini-batch—with an inclusion of an exponential moving average (EMA) with configurable decay,but we went for the most robust option and used percentiles statistics instead. We were inspired by the *return* rescaling mechanism presented in DreamerV3 [24]. Percentiles are indeed more robust statistics (*e.g.*, against outliers) compared to mean and standard deviation. We operate as follows.

First we divide the batch of rewards r by $\text{Perc}_{0.95}(r) - \text{Perc}_{0.05}(r)$, the gap between the 5th percentile of the batch and the 95th. Then, we shift the reward by $\text{Perc}_{0.05}(r)$ to re-center. We do not use an EMA. Despite its potential stabilization benefits, it exposes the method to rely too much on older statistics, thereby slowing down the method relatively to the other approaches. Note, since the percentiles are computed on the batch, the batch size hyper-parameter can not be too small. Picking a batch size below 16 for example would be ill-advised and could lead to degenerate cases. On the flip side, such a scheme is well-adapted to vectorized environments, where data collection is parallelized, and the batch size can usually be scaled up. We do not use a temperature hyper-parameter in the exponential of the reward.

In RND [9], the authors divide the operand of the exponential (like in our case, used to turn the negative loss into a positive reward signal) by a running average of the standard deviation. This statistic plays of the role of temperature. We hypothesize that this technique works well for RND because the reward is used as a reward bonus, aiming at better RL exploration. The method does not

care too much about which of two novel states is the most novel, as long as the agent does explore novel states. It is however of primary importance in our case, which could explain why this technique did not lead to good results in our early experiments.

In RED [61], the authors use a different hard-coded temperature for every environment. The temperature ranges from $\tau = 250$ to $\tau = 250,000$. In SECTION 5, we show results for our implementation of RED, and we apply the adaptive reward treatment described above instead of an unfair tuning of temperature τ per environment.

K CUDA Graphs

We use CUDA Graphs[8] in all the algorithms ran in the context of this work. CUDA Graphs optimize GPU workloads by capturing a **static** sequence of operations (*e.g.*, computations and memory transfers) into a *graph* that can be *replayed* with minimal overhead. **We generally gained a *3x* speedup on every workflow**, with extra precaution taken to ensure our PyTorch computational graphs were *static*, *i.e.* no conditional behavior based on the value of a tensor in the graph, etc.

L Implementation Details

All the methods tested in the work share the same actor-critic architecture, for fairness. The reward networks also align in terms of number of parameters, activations, initializations, etc. **Only DiffAIL** adopts a **different reward network** because it is a diffusion model. For DiffAIL [60] however, we took the authors' official implementation of the reward learning process, and made modifications to prevent pervasive NaN occurrences. Specifically, we replaced Mish activations with LeakyReLU, and added ϵ padding to the operands of logarithms and denominators. We left the DiffAIL reward architecture untouched otherwise, despite being deeper than those used in other methods. We posited that this would give the diffusion model a fairer chance, despite being misaligned with the rest.

We use the Adam optimizer [36] for all experiments.

M Main Environments

We report below the dimensionalities of the state and action spaces for the continuous control tasks considered in this work, based on the Gymnasium MuJoCo v4 environments documentation [58].

N Ablation Studies

To better understand the design choices underlying our method, we conducted a comprehensive set of ablation studies. These experiments span four random seeds and varying numbers of expert demonstrations, **totaling 92 training runs**. The results, summarized below, provide further empirical support for the architectural and algorithmic decisions presented in the main paper.

We first assess the contribution of the **histogram loss** "Gaussian type" ℓ_{HLG} by replacing it with a Mean Squared Error (MSE) Softmax loss on the Humanoid environment—the output embeddings returned by the predictor network f_ξ and prior network $f_\xi^\dagger$ are first wrapped with a softmax, before being compared with the MSE. As shown in FIGURE 4, the MSE Softmax loss fails to produce meaningful learning signals, leading to poor policy performance. In contrast, the histogram loss ℓ_{HLG} loss enables successful and stable training on this challenging high-dimensional benchmark.

Next, we evaluate the generalization capacity of the histogram loss ℓ_{HLG} across environments with *lower* state-action dimensionality the Humanoid. As illustrated in FIGURE 5, ℓ_{HLG} replicates the optimal results reported in the main text for non-Humanoid environments, albeit requiring different hyperparameter settings (for ℓ_{HLG}) than the Humanoid. In particular, the number of bins N, support width a and b, and Gaussian smoothing factor σ must be adapted to the environment. This supports the heuristic that these parameters should **scale with task difficulty**, in a manner similar to entropy target scaling in SAC [23]. The histogram loss is therefore able to make NGT optimal in more than

---

[8]https://pytorch.org/blog/accelerating-pytorch-with-cuda-graphs/

Table 1: Default Hyper-parameters for NGT Algorithm

Hyper-parameter	Default Value
GPU	True
PyTorch's `compile`	False
`CudaGraphs`	True
Number of parallel environments	4
Action repeat	1
Observation normalization	False
Number of environment steps	10^7
Learning starts at timestep	0
Evaluation steps	10
Evaluate every	10000
Evaluation window buffer size	20
Clip norm actor	20.0
Replay buffer size ($|\mathcal{D}|$)	4×10^6
Minibatch size ($|\mathcal{B}|$)	256
Discount factor (γ)	0.99
Polyak target smoothing coefficient (τ)	0.005
Learning rate – policy	3×10^{-4}
Learning rate – Q-networks	1×10^{-3}
Temperature parameter (α) – auto-tune	True
Temperature parameter (α) – initial value	0.2
Target entropy ($\mathcal{H}$)	$-|\mathcal{A}|$ (dimension of the action space)
Number of gradient steps per update	1
Number of environment steps per update	1
Learning rate – reward	1×10^{-3}
Spectral normalization	True
Gradient penalty	False
Output embedding size	32
Output post-`tanh` rescale	5.0
ℓ_{HLG} – Support $[a, b]$	$[-1, 1]$
ℓ_{HLG} – Number of bins N	21
ℓ_{HLG} – agent-side σ	0.05
ℓ_{HLG} – expert-side σ	0.25
Number of behavioral cloning iterations	10^7

Table 2: Dimensionalities of the state and action spaces for selected Gymnasium environments. These environments are commonly used benchmarks for continuous control in reinforcement learning.

Environment	State Dim.	Action Dim.
Ant-v4	111	8
HalfCheetah-v4	17	6
Pusher-v4	23	7
Walker2d-v4	17	6
Humanoid-v4	376	17

just the `Humanoid`; we just prioritized the use of pairing losses ℓ **without hyper-parameters** unless required. Hence, in the results reported in SECTION 5, we only used ℓ_{HLG} for the `Humanoid`.

We also ablate the **initialization scheme** used for the output embedding layers of the prior and predictor networks. As seen in FIGURE 6, switching from **orthogonal** initialization [53] to Kaiming initialization [27] introduces significant training instability and reduced performance. These results highlight the importance of initialization in preserving gradient flow and inducing stable dynamics in
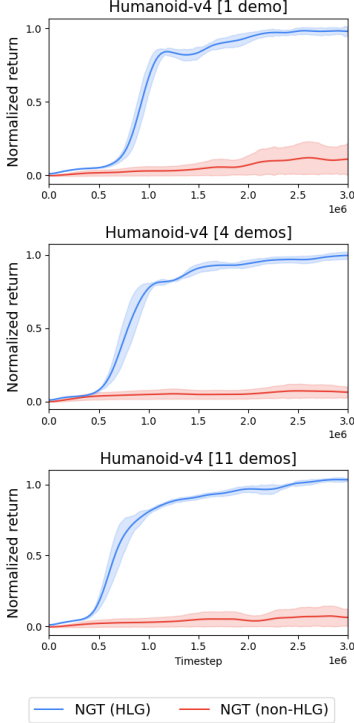
Figure 4: Comparison of the histogram loss ℓ_{HLG} and a Mean Squared Error (MSE) Softmax loss in NGT on the `Humanoid` environment. The MSE variant fails to yield meaningful learning, while ℓ_{HLG} enables successful and stable training.

the learned reward model. We refer the reader to SECTION 4.3.1 where we justify the design choice of opting for orthogonal initialization for the output embedding of the prior network $f_\xi^\dagger$.

Another critical component is **spectral normalization**. We remove spectral normalization from the prior and predictor networks and observe a complete failure of training, as reported in FIGURE 7. This indicates that constraining the Lipschitz constant of these networks is essential for stable and reliable reward learning. Note, **gradient penalization was not required**, unlike for DAC/SAM [8].

Finally, we study the impact of the output embedding dimensionality in the reward model by varying it across $\{8, 16, 32, 64\}$. As shown in FIGURE 8, performance is relatively stable for sizes 16 and above, but **degrades substantially** for 8-dimensional embeddings. This suggests that excessively compressing the output representation harms expressiveness and impedes optimization.

Taken together, these ablations substantiate the design principles of our approach and further validate the empirical findings presented in the main paper.
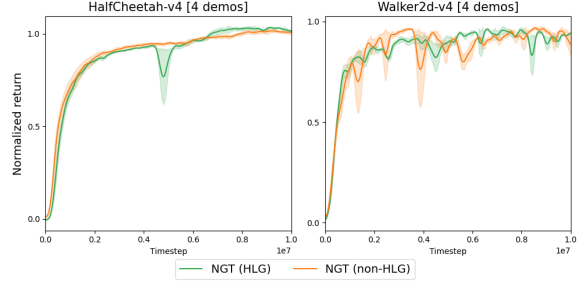
Figure 5: Performance of the histogram loss ℓ_{HLG} on non-`Humanoid` environments. Optimal results are recovered when adapting hyper-parameters such as support width, number of bins, and smoothing factor σ, highlighting the need for environment-specific scaling.
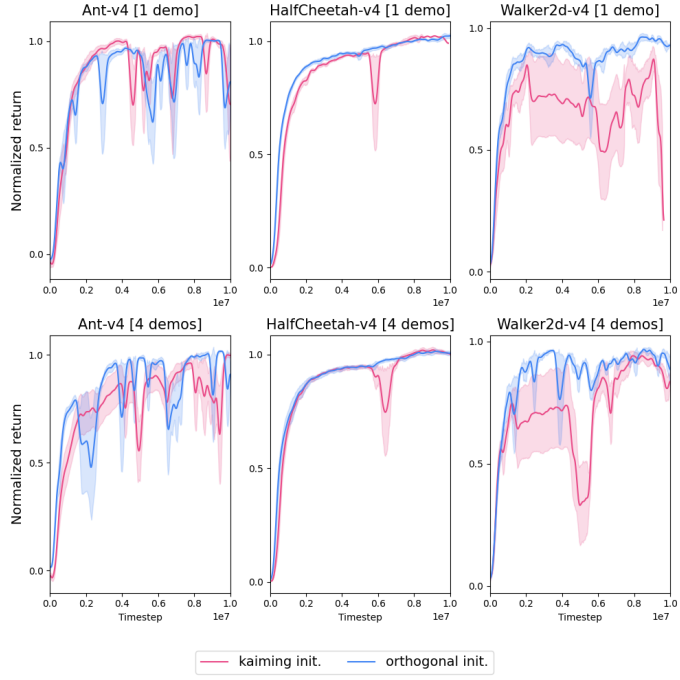

Figure 6: Impact of output embedding initialization scheme. Orthogonal initialization leads to higher stability and performance, whereas Kaiming initialization results in degraded learning and increased instability.
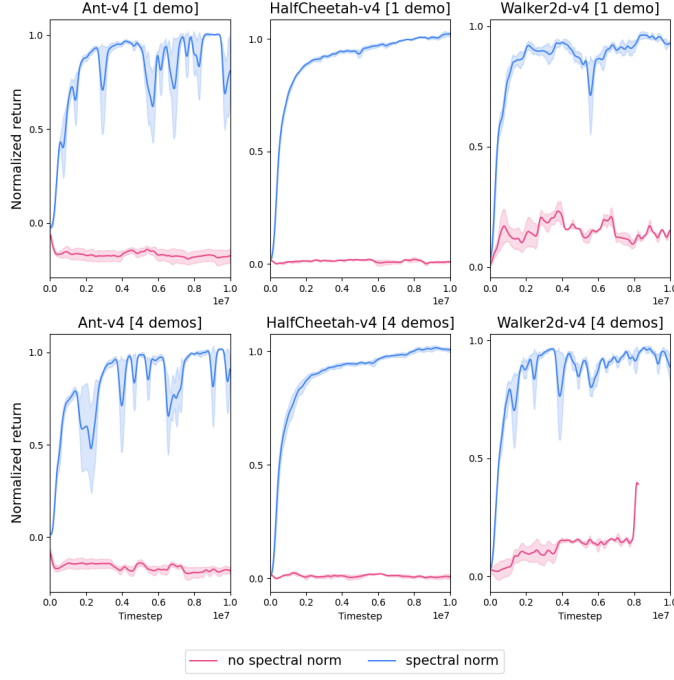
Figure 7: Effect of removing spectral normalization from the reward model's prior and predictor networks. Training becomes unstable and collapses completely, underscoring the necessity of spectral normalization for stable optimization.
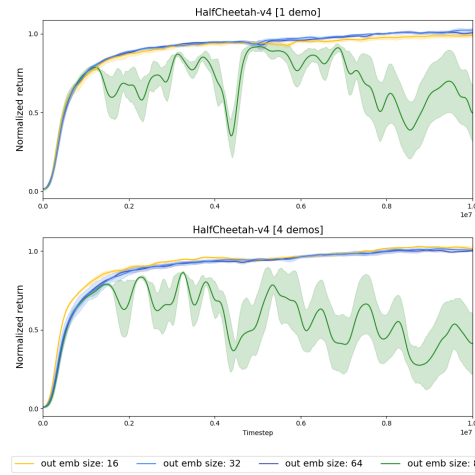

Figure 8: Effect of output embedding dimensionality in the reward model. Performance is robust for sizes 16, 32, and 64, but degrades significantly at dimension 8.
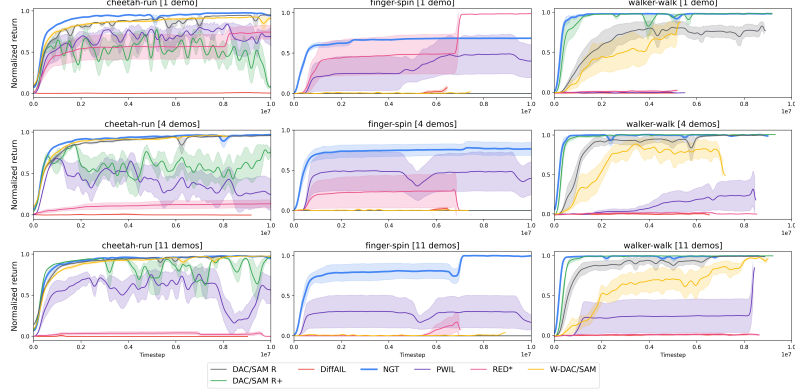
Figure 9: Performance of NGT and baseline methods on three DeepMind Control Suite tasks over various environments and numbers of demonstrations. DMC environments introduce greater variability in the initial state distribution, providing a more stringent test of generalization. NGT achieves strong and stable returns across all tasks, demonstrating robustness to increased stochasticity and variation in starting conditions.

O   Extra Environments

To further evaluate the robustness and generalization capacity of imitation learning agents, we extend our experiments to three environments from the DeepMind Control Suite (DMC) [57]: `walker-walk`, `cheetah-run`, and `finger-spin`. Compared to Gymnasium tasks, DMC environments exhibit **greater stochasticity in their initial state distributions**. This increased variability poses a significantly **harder generalization challenge**, as agents must adapt to a broader range of starting conditions rather than overfitting to narrow behavioral modes. This makes DMC a natural and meaningful extension for benchmarking IL methods, particularly in the **low-data regime**. Agents must not only mimic expert behavior but generalize it across unseen trajectories and perturbed states—highlighting the inductive biases and stability of the learning algorithm.

FIGURE 9 shows performance curves for NGT and several baseline methods across these three DMC tasks. We observe that NGT consistently achieves strong returns and exhibits remarkable training stability. In contrast, baseline methods often show high variance or fail to approach expert behavior at all, failing to generalize effectively under the broader initial state distributions. These results **further validate the generalization ability and sample efficiency of NGT** in more challenging, high-variance control settings.

P Speeds

We report the computational speed of the imitation learning methods we compare in SECTION 5, measured in **steps per second** (sps) at 200k environment time-steps. This allows us to assess their efficiency on two high-dimensional continuous control tasks: `Humanoid-v4` and `Walker2d-v4`.

Since the reported speeds are expressed in steps per second, **higher is better**.

Table 3: Speed (steps per second) of compared methods at 200k time-steps.

Method	Humanoid	Walker2d
PWIL	631	749
DiffAIL	659	929
DAC/SAM	741	953
MMD-DAC/SAM	749	977
W-DAC/SAM	763	978
NGT	**712**	**967**

`RED*` exhibits runtime performance on par with NGT.

NGT demonstrates competitive runtime efficiency with near-horizontal speed curves by 200k time-steps in both environments. This suggests that its performance stabilizes early, avoiding the degradation seen in other methods. DiffAIL, by contrast, exhibits a noticeable drop in speed over time, indicative of its steeper negative slope and greater runtime overhead. `DAC/SAM` achieves high speeds overall, though its reliance on gradient penalization introduces an initial computational burden. Nevertheless, by 200k steps, its speed curve also flattens, similar to NGT. PWIL is significantly slower, reflecting its less efficient reward computation. Among all methods, `MMD-DAC/SAM` and `W-DAC/SAM` are the fastest by a small margin, particularly in the more demanding `Humanoid-v4` task.

Overall, the results show that **NGT maintains a strong balance between computational efficiency and learning performance**, with speed profiles comparable to the fastest baseline methods while avoiding the pitfalls of runtime degradation.